Journal of Nano- and Electronic Physics
Vol. **18** No 5, 05009(5pp) (2026)

Журнал нано- та електронної фізики
Том **18** № 5, 05009(5cc) (2026)

OPEN ACCESS

REGULAR ARTICLE

Temperature-Dependent Spectral Characteristics of AlGaInP Quantum-Well Light-Emitting Diodes

O.I. Kyrylenko[1,*], R.M. Vernydub[1], T.M. Zahorodnia[2], D.P. Stratilat[3], V.P. Tartachnyk[1,3]

[1] *Dragomanov Ukrainian State University, 02000 Kyiv, Ukraine*
[2] *Sumy State University, 40007 Sumy, Ukraine*
[3] *Institute for Nuclear Research, National Academy of Sciences of Ukraine, 02000 Kyiv, Ukraine*

(Received 23 May 2026; revised manuscript received 18 October 2026; published online 28 October 2026)

The spectral characteristics of light-emitting diodes (LEDs) based on quaternary AlGaInP compounds incorporating quantum wells were investigated in the temperature range of 77-290 K using electroluminescence spectroscopy. At 77 K, the peak emission wavelength was $\lambda_{max} = 571$ nm, while the full width at half maximum (FWHM) of the emission band was 9 nm. Lorentzian and Gaussian line-shape functions were fitted to the experimental spectra in order to analyze the dominant broadening mechanisms. It was found that the Lorentzian profile provides better agreement with the measured spectra, indicating the predominance of homogeneous broadening in the investigated structures. The dependences of the emission intensity and the emission peak position on the injection current at 77 K were determined. The Urbach energy was evaluated from the slope of the low-energy tail of the electroluminescence spectra, whereas the carrier temperature was estimated from the high-energy side using the Boltzmann distribution. The temperature dependence of the Urbach energy was found to be linear, allowing the electron-phonon coupling coefficient to be determined as $g = 0.034$. The carrier temperature was shown to increase with injection current and to exceed the lattice (package) temperature because high-energy carriers preferentially overcome the potential barrier in the active region. The obtained results provide insight into the recombination processes and spectral broadening mechanisms in AlGaInP quantum-well LEDs and may be useful for improving the performance of visible-spectrum optoelectronic devices.

Keywords: AlGaInP LEDs, Quantum wells, Electroluminescence spectra, Urbach energy, Carrier temperature, Electron-phonon interaction, Spectral broadening.

DOI: 10.21272/jnep.18(5).05009 PACS numbers: 78.60.Fi, 73.21.Fg

1. INTRODUCTION

Modern high-efficiency AlGaInP light-emitting diodes (LEDs) are fabricated using quaternary solid solutions of the composition $(Al_xGa_{1-x})_{0.5}In_{0.5}P$. Their emission wavelength can be tuned from red ($\lambda_{max} = 626$ nm) through orange ($\lambda_{max} = 610$ nm) to yellow ($\lambda_{max} = 590$ nm) by varying the Al/Ga composition ratio x. An increase in "x" shifts the emission spectrum toward shorter wavelengths; however, at $x \approx 0.53$ the material undergoes a transition to an indirect band-gap semiconductor, resulting in a significant reduction in the radiative efficiency for wavelengths below 570 nm [1, 2].

Despite the high internal quantum efficiency (IQE) of AlGaInP LEDs in the direct-band-gap region (approaching 100 %), their external quantum efficiency (EQE) remains considerably lower, typically within 5-7 %. This reduction is mainly caused by the high refractive indices of the materials forming the complex multilayer structure and by multiple internal reflections at the interfaces. Consequently, only a narrow cone of emitted light escapes the device, accounting for approximately 10 % of the total generated radiation [3].

Quaternary AlGaInP materials exhibit excellent lattice matching with GaAs substrates, thereby minimizing the formation of misfit dislocations. However, GaAs possesses relatively low thermal conductivity and limited transparency in the visible spectral range, which hinders both light extraction and heat dissipation. In contrast, GaP substrates are transparent, but the substantial lattice mismatch between AlGaInP and GaP leads to increased densities of threading dislocations and residual strain during epitaxial growth [4]. Therefore, a compromise must be found between structural quality and efficient light extraction.

The primary factors limiting the external efficiency of AlGaInP LEDs are non-radiative recombination processes and photon recycling within the active region [5].

The influence of self-heating effects can be partially compensated by operating the devices in a submicrosecond pulsed mode [6].

As demonstrated in [7], the external quantum efficiency of AlGaInP LEDs decreases with decreasing device size due to enhanced sidewall losses, while the ideality factor increases from 1.47 to 1.95. Furthermore, small-sized LEDs containing five quantum wells (QWs) exhibit approximately 30 % higher IQE than devices incorporating twenty quantum wells.

* Correspondence e-mail: o.i.kyrylenko@udu.edu.ua

© 2026 The Author(s). Journal of Nano- and Electronic Physics published by Sumy State University. This article is distributed under the terms and conditions of the Creative Commons Attribution (CC BY) license.

Cite this article as: O.I. Kyrylenko et al., *J. Nano- Electron. Phys.* 18 No 5, 05009 (2026) https://doi.org/10.21272/jnep.18(5).05009

The development of high-quality display technologies requires efficient full-color RGB LEDs with low power consumption [8]. High-brightness AlGaInP micro-light-emitting diodes (μLEDs) are considered promising candidates for such applications [9]. However, their major drawback is the large surface-to-volume ratio, which results in increased leakage currents.

At present, dangling surface bonds are commonly compensated through surface passivation by depositing appropriate dielectric films on μLED structures [10].

Red LEDs play a crucial role in generating white light. Compared with InGaN-based counterparts, AlGaInP LEDs exhibit higher brightness, narrower emission bandwidths, and the absence of strong polarization fields [11].

The degradation of AlGaInP LED characteristics is associated with dark-spot defects arising from metal diffusion from contacts, compositional fluctuations, recombination-enhanced defect generation, and other mechanisms. These degradation processes are intensified under electrothermal stress conditions. It has been shown that the degradation rate of optical output power in AlGaInP LEDs is lower than that observed in typical InGaN LEDs [12].

The application range of LED radiation sources extends from advanced photonic devices to everyday consumer technologies [13]. Emitters based on quaternary compounds have found widespread use in full-color displays and are considered highly promising for next-generation high-resolution display technologies [14-18].

An example of the biomedical application of AlGaInP LEDs is presented in [19], where a miniature sensor capable of real-time object detection was proposed for surgical and portable medical systems. The integrated microsensor can detect force vectors as low as 1 mN within the ranges of 0 – 20 mN for normal forces and 0 – 15 mN for tangential forces, while occupying an area of only 1.5 mm^2.

Based on the literature review presented above, the aim of this work was to perform a detailed analysis of the low-temperature emission spectra of AlGaInP LEDs, determine the principal optical and injection characteristics of their spectral lines in the temperature range 77-290 K, and evaluate the electron-phonon coupling coefficient.

2. EXPERIMENT

Spectral measurements were performed using a Green-Wave digital spectrometer (350 – 1150 nm, StellarNet, USA). The investigated samples were AlGaInP-based light-emitting diodes containing quantum wells. The measurements were carried out in the temperature range of 77-290 K at a constant injection current of I = 20 mA.

3. RESULTS AND DISCUSSION

The results of optical characterization of AlGaInP LEDs with quantum wells are presented below. The peak emission wavelength at 77 K was λ_{max} = 571 nm, while the full width at half maximum (FWHM) of the emission band was 9 nm (Γ = 4.5 nm). Fig. 1 shows the electroluminescence spectra recorded at different temperatures in the range of 77-290 K under a forward current of I = 20 mA.

For each spectrum, classical Lorentzian and Gaussian distributions were also calculated. For spectroscopic applications, they can be expressed as:

$$f_L(x) = \frac{1}{\pi} \frac{\Gamma}{(x-x_0)^2+\Gamma^2},$$

$$f_G(x) = \frac{1}{\sigma\sqrt{2\cdot\pi}} exp\left\{-\frac{(x-\mu)^2}{2\sigma^2}\right\},$$

where x_0 denotes the spectral peak position, Γ is the half-width at half maximum (HWHM), with FWHM = 2Γ, and σ and μ are parameters defining the line profile.

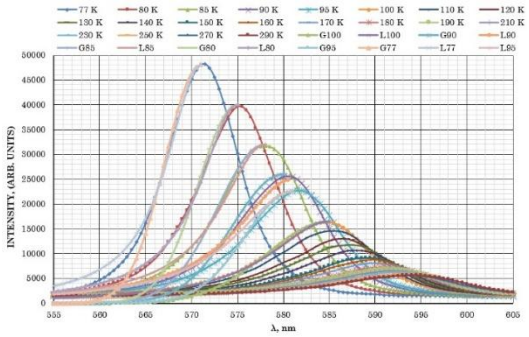


Fig. 1 – Electroluminescence spectra of AlGaInP quantum-well LEDs measured in the temperature range 77-290 K at a forward current of I = 20 mA. Solid lines represent Lorentzian (L) and Gaussian (G) fits

Lorentzian and Gaussian functions are the most common distributions used in optical spectroscopy. Under identical conditions, the Lorentzian profile exhibits a sharper peak and more pronounced wings than the Gaussian profile. The degree of spectral line broadening is characterized by its width. According to the Heisenberg uncertainty relation,

$$\Delta\varepsilon \cdot \Delta\tau \approx \hbar$$

The linewidth of an optical transition includes the so-called natural (radiative) broadening. When the lifetime of the excited state is short ($\Delta t \to 0$), the energy width $\Delta\varepsilon$ becomes large. Taking into account that $\Delta\varepsilon = \hbar\omega$, one obtains the fundamental relation of spectral analysis:

$$\Delta\varepsilon \cdot \tau \cong 1$$

States with long lifetimes τ are characterized by narrow spectral lines, whereas short-lived states produce broader lines. The natural linewidth is typically very small and is determined by the finite lifetime of the excited state.

Line broadening is referred to as homogeneous when the spectral lines of all individual atoms or emitters broaden equally. Examples include natural broadening and collision (pressure) broadening, which originates from atomic collisions and is well described by the Lorentzian distribution. Broadening caused by the Doppler effect or by atomic disorder within a crystal lattice is generally described by the Gaussian distribution.

In cubic crystals, homogeneous broadening predominates; therefore, Lorentzian line profiles are expected. The closer the crystal structure is to an ideal cubic lattice, the smaller the contribution of inhomogeneous broadening to the overall linewidth.

A slight discrepancy between the experimental and fitted spectra is observed only in the lower-energy portions of the spectral lines. Toward the wings of the distributions, the difference between the experimental spectrum and both Lorentzian and Gaussian profiles becomes more pronounced.

The Lorentzian function reproduces the experimental line shape more accurately than the Gaussian function, whereas the latter decreases too rapidly and does not adequately reproduce the spectral wings.

The low-energy tail of the emission spectrum can be described by an exponential Urbach-type dependence:

$$I(h\nu) \sim \exp\left(\frac{h\nu - E_0}{E_U}\right), \quad (1)$$

where E_U is the Urbach energy and E_0 is a characteristic energy, usually close to the band-gap energy E_g, corresponding to the inflection point of the spectrum.

The Urbach energy (E_U) characterizes the degree of structural disorder in a crystal and determines the width of the exponential tail of the density of states. Lower values of E_U indicate a higher crystal quality.

For high-quality A^{III}-B^{V} semiconductor compounds at 300 K, typical values are:

$$E_U{}^{GaAs} = 5.9 - 7.5 \text{ meV};$$

$$E_U{}^{InP} = 7.1 \text{ meV};$$

$$E_U{}^{GaP} = 10 - 15 \text{ meV};$$

$$E_U{}^{GaN} = 15 - 40 \text{ meV}.$$

The E_U is significantly larger in InGaN alloys, $E_U{}^{InGaN} = 20 - 60$ meV due to alloy-composition fluctuations associated with indium-rich clusters. It increases with increasing indium content and may reach values as high as 90−100 meV [20, 21].

According to Eq. (1), the E_U can be determined from the slope of the low-energy side of the emission spectrum. Analysis of emission spectra is particularly convenient because it enables the determination of this important parameter directly under operating conditions.

For AlGaInP layers lattice-matched to GaAs substrates, $E_U{}^{AlGaInP} = 2 - 10$ meV at 300 K. As the aluminum content (x) increases, the value of $E_U{}^{AlGaInP}$ also increases. Spontaneous ordering of atoms in the group-III sublattice reduces the $E_U{}^{AlGaInP}$ to approximately 10−12 meV, whereas disordered alloys exhibit values of $E_U{}^{AlGaInP} = 18 - 25$ meV.

For the investigated samples, the temperature dependence of the Urbach energy was found to be linear (see Fig. 2):

$$E_U(T) = E_U(0) + \sigma \cdot kT,$$

where $E_U(0)$ is the contribution of static disorder and σ is the electron–phonon interaction parameter that determines the temperature-dependent slope of the absorption coefficient caused by electron-phonon interaction [22]. The electron-phonon coupling constant is defined as $g = \frac{2}{3\sigma}$.

Fig. 2 shows that the slope of the $E_U(T)$ dependence within the temperature range of 80-100 K is approximately $\frac{5}{3}10^{-3}$eV, because $\sigma \cdot K = \frac{5}{3}10^{-3}$eV This yields $\sigma = 19.33$ and $g = 0.034$.

Weak electron-phonon coupling ($g < 0.5$) is characteristic of conventional metallic systems, whereas larger values of g are typically associated with strong electron-phonon interactions and may indicate conditions favorable for superconductivity. The relatively large value of (g) obtained in this work may indicate the influence of ballistic carrier transport through the active region of the LED.

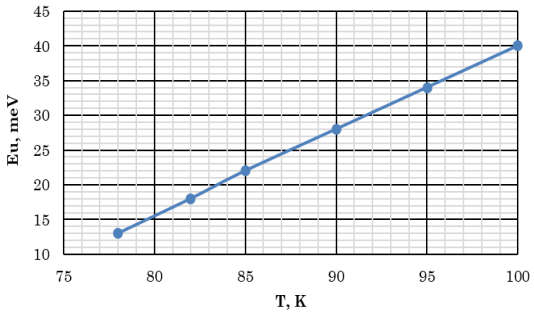


Fig. 2 – Temperature dependence of the Urbach energy of the AlGaInP LED measured at $I = 20$ mA ($\lambda_{max} = 590$ nm)

Heating of LEDs due to environmental conditions and current flow leads to changes in optical power characteristics and adversely affects the peak emission wavelength, internal efficiency, operational lifetime, and reliability. These degradation mechanisms are associated with accelerated dislocation migration and impurity diffusion, which may destroy excitonic recombination centers.

One of the most accurate methods for determining carrier temperature (T_e) is the use of a temperature sensor integrated directly into the LED package [25]. For high-power emitters, carrier temperature can also be estimated from temperature-dependent current–voltage characteristics [26] or from the nonlinear voltage–temperature relationship [27].

In the present work, we employed the spectral method proposed in Ref. [24]. According to this approach, the recombination emission intensity follows the Boltzmann distribution:

$$I_{int} \sim \exp\left[-\frac{h\nu}{kT_e}\right]$$

where T_e is the carrier temperature. Therefore, the slope of the high-energy side of the emission spectrum determines the carrier temperature:

$$\frac{d(\ln I_{int})}{d(h\nu)} \sim -\frac{1}{kT_e}.$$

Calculations based on the spectra presented in Fig. 1 showed that for currents in the range of 10-25 mA, the carrier temperature is $T_e = 148$ K, whereas for currents of 30-75 mA it increases to $T_e = 195$ K. Consequently, the temperature T_e differences between the carriers and the package maintained at 77 K are $\Delta T_1 = 71$ K and $\Delta T_2 = 118$ K, respectively.

The dependence of the carrier temperature T_e on the package temperature is shown in Fig. 3. It can be seen that at approximately $T = 95$ K the carrier temperature reaches a critical value for contact alloys.

Nevertheless, the LED retains its functional properties and remains suitable for repeated operation.

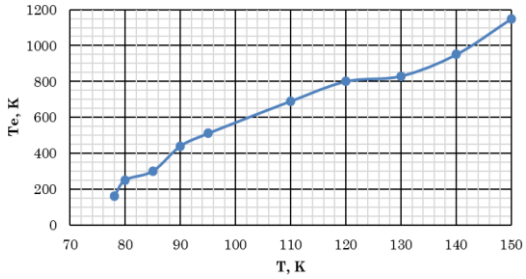


Fig. 3 – Dependence of carrier temperature Te on the ambient temperature of the AlGaInP LED measured at $I = 20$ mA ($\lambda_{max} = 590$ nm)

The actual junction temperature is therefore expected to be significantly lower than T_e, since the potential barrier is crossed preferentially by high-energy carriers.

4. CONCLUSIONS

It was found that, among the two classical line-shape functions, namely the Lorentzian and Gaussian distributions, the Lorentzian distribution provides the best agreement with the experimental electroluminescence spectra of AlGaInP LEDs. The temperature dependence of the Urbach energy of the LED active layer was shown to be linear. The electron-phonon coupling coefficient in the active-layer alloy was determined from the slope of the $E_U(T)$ dependence and was found to be ($g = 0.034$).

The carrier temperature (T_e) was calculated as a function of the ambient temperature surrounding the sample. It was also established that the carrier temperature exceeds the junction temperature due to the preferential transport of high-energy carriers across the potential barrier.

REFERENCES

1. V.I. Karas, L.A. Nazarenko, I.V. Karas, *Svitlodiody: fizyka, tekhnolohiia vyhotovlennia, zastosuvannia. Light-Emitting Diodes: Physics, Manufacturing Technology, Applications* (Kharkiv: KhNAMH: 2012).
2. Y.J. Lee, C.J. Lee, C.H. Chen, *Extended Abstracts of the 2010 International Conference on Solid State Devices and Materials* (Tokyo: The Japan Society of Applied Physics, The University of Tokyo: 2010) https://doi.org/10.7567/SSDM.2010.P-7-15.
3. W.-C. Cheng, S.-Y. Huang, Y.-J. Chen, C.-S. Wang, H.Y. Lin, T.-M. Wu, R.-H. Horng, *Sci. Rep.* **8**, 911 (2018) https://doi.org/10.1038/s41598-018-19405-y.
4. R.-H. Horng, B.-R. Wu, C.-F. Weng, P. Ravadgar, T.-M. Wu, S.-P. Wang, J.-H. He, T.-H. Yang, Y.-M. Chen, T.-C. Hsu, A.-S. Liu, D.-S. Wuu, *Opt. Exp.* **21**, 19668 (2013) https://doi.org/10.1364/OE.21.019668.
5. P. Altieri, A. Jaeger, R. Windisch, N. Linder, P. Stauss, R. Oberschmid, K. Streubel, *J. Appl. Phys.* **98**, 086101 (2005) https://doi.org/10.1063/1.2085308.
6. Yadav, I.E. Titkov, G.S. Sokolovskii, S.Yu. Karpov, V.V. Dudelev, K.K. Soboleva, M. Strassburg, I. Pietzonka, H.-J. Lugauer, E.U. Rafailov, *J. Appl. Phys.* **124**, 013103 (2018) https://doi.org/10.1063/1.5020266.
7. J.-T. Oh, S.-Y. Lee, Y.-T. Moon, J.H. Moon, S. Park, K.Y. Hong, K.Y. Song, C. Oh, J.-I. Shim, H.-H. Jeong, J.-O. Song, H. Amano, T.-Y. Seong, *Opt. Exp.* **26**, 11194 (2018) https://doi.org/10.1364/OE.26.011194.
8. B.O. Jung, W. Lee, J. Kim, M. Choi, H.-Y. Shin, M. Joo, S. Jung, Y.-H. Choi, M.J. Kim, *Sci. Rep.* **11**, 4535 (2021) https://doi.org/10.1038/s41598-021-83933-3.
9. M. Zhanghu, W. Huang, H. Yang, Y. Lin, Z. Wang, K. Wang, Z. Liu, *SID Symp. Digest Tech. Papers* **53**, 874 (2022) https://doi.org/10.1002/sdtp.16125.
10. T. Kim, S. Kim, P. Uthirakumar, Y.-H. Cho, P.-K. Jang, S. Baek, J. Park, I.-H. Lee, *Appl. Surf. Sci.* **688**, 162437 (2025) https://doi.org/10.1016/j.apsusc.2025.162437.
11. K. Fan, K. Zheng, J. Lv, B. Zhao, Y. Zhao, Y. Chen, Y. Qin, Q. Wang, W. Wang, J. Liang, *Opt. Exp.* **31**, 36293 (2023) https://doi.org/10.1364/OE.503024.
12. H. Chen, A. Keppens, P. Hanselaer, Y. Lu, Y. Gao, R. Zhuang, Z. Chen, *Semiconductors* **46**, 1310 (2012) https://doi.org/10.1134/S1063782612100041.
13. S.S. Li, *Semiconductor Physical Electronics* (New York: Springer New York: 2006) https://doi.org/10.1007/0-387-37766-2_13.
14. B. Choi, D.-H. Kim, D. Kang, T.-Y. Seong, *J. Alloy. Compd.* **699**, 1180 (2017) https://doi.org/10.1016/j.jallcom.2016.12.211.
15. R.-H. Horng, H.-Y. Chien, F.-G. Tarntair, D.-S. Wuu, *IEEE J. Electron Dev. Soc.* **6**, 1064 (2018) https://doi.org/10.1109/JEDS.2018.2864543.
16. S. Han, C. Xu, H. Li, S. Liu, H. Xu, Y. Zhu, A. Fang, X. Wang, *Opt. Mater.* **114**, 110860 (2021) https://doi.org/10.1016/j.optmat.2021.110860.
17. W. Guo, W. He, Z. Qi, J. Zhang, C. Tong, M. Li, J. Zhong, Y. Lu, T. Wu, Z. Chen, R. Zhang, *Prog. Quantum Electron.* **104**, 100598 (2025) https://doi.org/10.1016/j.pquantelec.2025.100598.
18. J. Ye, W. Su, Y. Lin, Y. Peng, X. Zhou, T. Guo, J. Yuan, J. Sun, Q. Yan, Y. Zhang, C. Wu, *Adv. Sci.* **12**, e11520 (2025) https://doi.org/10.1002/advs.202511520.
19. J. Feng, Z. Wang, M. Zhanghu, X. Zhang, Y. Shen, J. Yang, Z. Li, B. Chen, T. Wang, X. Chen, Z. Liu, *Microsyst. Nanoeng.* **10**, 85 (2024) https://doi.org/10.1038/s41378-024-00712-6.
20. M. Beaudoin, A.J.G. DeVries, S.R. Johnson, H. Laman, T. Tiedje, *Appl. Phys. Lett.* **70**, 3540 (1997) https://doi.org/10.1063/1.119226.
21. J.M. McMahon, D.S.P. Tanner, E. Kioupakis, S. Schulz, *Appl. Phys. Lett.* **116**, 181104 (2020) https://doi.org/10.1063/5.0006128.
22. V.Yu. Bihanych, I.Yu. Kurytsia, V.S. Shusta, O.I. Herzanych, *Nauk. Visnyk Uzhhorod. Univ. Ser. Fiz.* No 25, 45 (2009) https://dspace.uzhnu.edu.ua/jspui/handle/lib/14813.
23. S.M. Sichkar, *Usp. Fiz. Met.* **18**, 27 (2017) https://doi.org/10.15407/ufm.18.01.027.
24. E.F. Schubert, *Light-Emitting Diodes*, 2nd ed. (Cambridge: Cambridge University Press: 2006) https://doi.org/10.1017/CBO9780511790546.
25. S. Pan, C. Sun, Y. Zhou, W. Chen, R. Zhang, Y. Zheng, *Appl. Sci.* **10**, 444 (2020) https://doi.org/10.3390/app10020444.
26. Keppens, W.R. Ryckaert, G. Deconinck, P. Hanselaer, *J. Appl. Phys.* **104**, 093104 (2008) https://doi.org/10.1063/1.3009966.
27. Onwukaeme, W.-J. Choi, H.-Y. Ryu, *Opt. Quantum Electron.* **53**, 513 (2021) https://doi.org/10.1007/s11082-021-03182-6.

Температурно-залежні спектральні характеристики світлодіодів AlGaInP з квантовими ямами

О.І. Кириленко[1], Р.М. Вернидуб[1], Т.М. Загородня[2], Д.П. Стратілат[3], В.П. Тартачник[1,3]

[1] *Український державний університет імені Михайла Драгоманова, 02000 Київ, Україна*
[2] *Сумський державний університет, 40000 Суми, Україна*
[3] *Інститут ядерних досліджень, Національної академії наук України, 02000 Київ, Україна*

Досліджено спектральні характеристики світлодіодів (СД), виготовлених на основі четвертинних сполук AlGaInP із квантовими ямами, методом спектроскопії електролюмінесценції в температурному інтервалі 77-290 K. За температури 77 K довжина хвилі в максимумі випромінювання становила λ_{max} = 571 нм, а повна ширина смуги випромінювання на половині максимуму (FWHM) дорівнювала 9 нм. Для аналізу домінуючих механізмів спектрального розширення експериментальні спектри апроксимовано функціями розподілу Лоренца та Гауса. Встановлено, що профіль Лоренца краще узгоджується з експериментальними спектрами, що свідчить про переважання механізму однорідного розширення в досліджуваних структурах. Одержано залежності інтенсивності випромінювання та положення максимуму спектра від інжекційного струму за температури 77 K. Енергію Урбаха визначено за нахилом низькоенергетичної частини спектрів електролюмінесценції, тоді як температуру носіїв заряду оцінено за нахилом їх високоенергетичної частини відповідно до розподілу Больцмана. Встановлено лінійний характер температурної залежності енергії Урбаха, що дало змогу визначити коефіцієнт електрон-фононної взаємодії g = 0,034. Показано, що температура носіїв зростає зі збільшенням інжекційного струму та перевищує температуру кристалічної ґратки (корпусу) внаслідок переважного подолання потенціального бар'єра високоенергетичними носіями в активній області. Одержані результати поглиблюють розуміння рекомбінаційних процесів і механізмів спектрального розширення в світлодіодах AlGaInP із квантовими ямами та можуть бути використані для підвищення ефективності оптоелектронних пристроїв видимого спектрального діапазону.

Ключові слова: Світлодіоди AlGaInP, Квантові ями, Спектри електролюмінесценції, Енергія Урбаха, Температура носіїв заряду, Електрон-фононна взаємодія, Спектральне розширення.